Metal-triggered conformational reorientation of a self-peptide bound to a disease-associated HLA-B*27 subtype

Received for publication, April 19, 2019, and in revised form, July 8, 2019 Published, Papers in Press, July 11, 2019, DOI 10.1074/jbc.RA119.008937

Ronja Driller[‡1], Martin Ballaschk[§], Peter Schmieder[§], Barbara Uchanska-Ziegler[¶‖], Andreas Ziegler[‖2], and Bernhard Loll[‡**3]

*From the [‡]Institut für Chemie/Biochemie, AG Strukturbiochemie, Freie Universität Berlin, Takustrasse 6, 14195 Berlin, Germany, the [§]Leibniz-Institut für Molekulare Pharmakologie, Robert-Rössle-Strasse 10, 13125 Berlin, Germany, the [¶]Institut für Immungenetik, Charité-Universitätsmedizin Berlin, Freie Universität Berlin, Thielallee 73, 14195 Berlin, Germany, [‖]Ziegler Biosolutions, Fahrgasse 5, 79761 Waldshut-Tiengen, Germany, and **MoloX GmbH, Takustrasse 6, 14195 Berlin, Germany*

Edited by Peter Cresswell

Conformational changes of major histocompatibility complex (MHC) antigens have the potential to be recognized by T cells and may arise from polymorphic variation of the MHC molecule, the binding of modifying ligands, or both. Here, we investigated whether metal ions could affect allele-dependent structural variation of the two minimally distinct human leukocyte antigen (HLA)-B*27:05 and HLA-B*27:09 subtypes, which exhibit differential association with the rheumatic disease ankylosing spondylitis (AS). We employed NMR spectroscopy and X-ray crystallography coupled with ensemble refinement to study the AS-associated HLA-B*27:05 subtype and the AS-non-associated HLA-B* 27:09 in complex with the self-peptide pVIPR (RRKWRRWHL). Both techniques revealed that pVIPR exhibits a higher degree of flexibility when complexed with HLA-B*27:05 than with HLA-B*27:09. Furthermore, we found that the binding of the metal ion Cu^{2+} or Ni^{2+}, but not Mn^{2+}, Zn^{2+}, or Hg^{2+}, affects the structure of a pVIPR-bound HLA-B*27 molecule in a subtype-dependent manner. In HLA-B*27:05, the metals triggered conformational reorientations of pVIPR, but no such structural changes were observed in the HLA-B*27:09 subtype, with or without bound metal ion. These observations provide the first demonstration that not only major histocompatibility complex class II, but also class I, molecules can undergo metal ion–induced conformational alterations. Our findings suggest that metals may have a role in triggering rheumatic diseases such as AS and also have implications for the molecular basis of metal-induced hypersensitivities and allergies.

The association of the human leukocyte antigen (HLA)[4] *HLA-B*27* with rheumatic disorders, in particular ankylosing spondylitis (AS), has been known for nearly 50 years, but the underlying reasons have remained enigmatic (1, 2). Because only a small fraction of *HLA-B*27*–positive individuals develop AS, other factors, genetic as well as environmental, have to contribute to initiate disease (3–6). An understanding could come from functional, biochemical, and biophysical studies of *HLA-B*27* subtypes with differential AS association (7, 8). We have previously analyzed the subtypes *HLA-B*27:05* (in short, *B*27:05*) and *HLA-B*27:09* (in short, *B*27:09*), which are distinguished by only a single amino acid exchange at heavy chain (HC) position 116 (Asp in B*27:05, His in B*27:09) at the floor of the binding groove. The former variant is disease-associated, whereas *B*27:09* is not.

Despite the close subtype relatedness, healthy *B*27:05*-positive individuals and AS patients in particular possess cytotoxic T lymphocytes (CTL) in abundance that recognize the self-peptide pVIPR (RRKWRRWHL, derived from vasoactive intestinal peptide type 1 receptor residues 400–408), whereas such effector cells are very rare in individuals with *B*27:09* (9, 10). This indicates that the elimination of pVIPR-specific, self-reactive CTL during thymic selection processes is impaired in persons with the AS-associated subtype. Structural studies of the pVIPR-HLA-B*27 complexes revealed that pVIPR is displayed differentially by the two subtypes: B*27:09 presents the peptide conventionally in the canonical conformation (CC), with its middle bulging out of the binding groove (Fig. 1*A*), whereas the B*27:05 subtype displays pVIPR in a highly unusual dual conformation, about half resembling the CC structure seen in B*27:09 and the other half in a noncanonical conformation (NC), with the middle of the peptide contacting the polymorphic HC residue 116 (Fig. 1*B*). These results suggested that structural peculiarities were responsible for the differential recognition of the two subtypes by T cells and their difference in disease association (9).

This work was supported by the Forschungskommission of the Freie Universität Berlin, the Fonds der Chemischen Industrie, the Leibniz-Institut für Molekulare Pharmakologie (FMP), Deutsche Forschungsgemeinschaft (Bonn-Bad Godesberg, Germany) Grants SCHM880/9-1 and UC8/2-1), Volkswagen Stiftung (Hannover, Germany) Grant I/79989, and the Fondazione Ceschina (Lugano, Switzerland) (to A. Z.). The authors declare that they have no conflicts of interest with the contents of this article.

The atomic coordinates and structure factors (codes 5IB1, 5IB2, 5IB3, 5IB4, and 5IB5) have been deposited in the Protein Data Bank (http://wwpdb.org/).

[1] Supported by Elsa-Neumann and Nüsslein-Volhard stipends.

[2] To whom correspondence may be addressed: Ziegler Biosolutions, Fahrgasse 5, 79761 Waldshut-Tiengen, Germany. Tel.: 49-7741-969-0722; E-mail: ziegler-biosolutions@gmx.de.

[3] To whom correspondence may be addressed: Institut für Chemie/Biochemie, AG Strukturbiochemie, Freie Universität Berlin, Takustrasse 6, 14195 Berlin, Germany. Tel.: 49-30-838-57348; Fax: 49-30-838-457348; E-mail: loll@chemie.fu-berlin.de.

[4] The abbreviations used are: HLA, human leukocyte antigen; β_2m, β_2-microglobulin; HC, heavy chain; MHC, major histocompatibility complex; AS, ankylosing spondylitis; CTL, cytotoxic T lymphocytes; CC, canonical conformation; NC, non-canonical conformation; RT, room temperature; TCR, T cell receptor; Fmoc, *N*-(9-fluorenyl)methoxycarbonyl; MD, molecular dynamics; HMQC, heteronuclear multiple-quantum correlation.

However, subsequent analyses by IR spectroscopy and molecular dynamics (MD) simulations revealed the existence of elevated conformational flexibility in the AS-associated subtype B*27:05, whereas the B*27:09 HC was less mobile (11–14). Furthermore, an analysis of another pair of nearly identical HLA-B*27 subtypes, B*27:04 (AS-associated) and B*27:06 (not AS-associated), demonstrated that the former subtype, presenting pVIPR in a single CC conformation, was more flexible than B*27:06, although this subtype displayed pVIPR in a dual conformation, one of them in CC and the other in NC-binding mode (15). These results imply that AS-associated HLA-B*27 subtypes are characterized by an increased conformational flexibility and that structural peculiarities, such as dual conformations of a presented peptide, may have no influence on initiating the disease.

A detailed understanding of the interdependence of subtype polymorphism, in particular at HC position 116, and conformational flexibility of a bound peptide cannot be obtained by conventional X-ray crystallography alone. We have therefore revisited our previous structural findings using NMR spectroscopy and X-ray crystallography in combination with classical maximum likelihood and ensemble refinement (16, 17). The first technique is known to yield very detailed information on the structure as well as the dynamics of a molecule, whereas classical X-ray crystallography provides atomic resolution without in-depth information on conformational flexibility. Ensemble refinement of crystallographic structures, on the other hand, seeks to bridge the gap between the two former techniques by including short, steered MD simulations, resulting in ensembles of structures for highly mobile residues. These novel experiments have led to a greatly improved understanding of differential peptide mobility in the B*27:05 and B*27:09 subtypes.

In addition, we can now demonstrate that the acquisition of the dual pVIPR conformation within the B*27:05 binding groove can be induced by selected metal ions that bind to exposed residues of the complex. The conformation of the same peptide bound to B*27:09 is, however, not affected. These findings have implications not only for the differential disease association of the *HLA-B*27* subtypes, but more generally, also for the molecular basis underlying metal-induced hypersensitivities and allergies.

Results

Peptide conformations analyzed by NMR spectroscopy

The conformational plasticity of the pVIPR peptide was initially assessed in both subtypes by NMR spectroscopy. Because the individual components of the MHC molecules are produced separately, the labeling pattern for each can be chosen independently. We have utilized this approach previously in an investigation in which solely β_2-microglobulin (β_2m) was labeled with ^{15}N and thus was the only component visible in the spectra. Two-dimensional ^{1}H,^{15}N correlations of good intensity and linewidth were recorded in that investigation in a comparatively short time (*i.e.* 1.5 h). For the NMR spectra recorded here, we employed samples containing ^{15}N,^{13}C-labeled Arg at positions 1, 2, 5, and 6 of the peptide in otherwise unlabeled complexes. The intensities and linewidth obtained in NMR spectra are independent of the labeling pattern. Thus, we expected to obtain spectra with peak shapes comparable with those of the samples where only β_2m was labeled. Judging from the previously obtained crystal structures (9), we expected ^{1}H,^{15}N correlations with three resonances for backbone H–N pairs as well as up to four H–N pairs for arginine side chains for pVIPR-B*27:09 and a double set of signals for pArg-5 and pArg-6 in pVIPR-B*27:05, due to the double conformation of the peptide (pArg-1 and pArg-2 are identically bound in both subtypes; Fig. 1, *A* and *B*). In contrast, we found that the resonance lines were broadened for both complexes, indicating conformational exchange on the microsecond to millisecond time scale. These broad lines made long experiment times necessary (20 h instead of 1.5 h). More importantly, whereas pVIPR-B*27:09 (Fig. 1*C*) showed the expected pattern in the ^{1}H,^{15}N correlation, the spectrum of pVIPR-B*27:05 (Fig. 1*D*) did not contain the expected double set of signals, suggesting the presence of a different, most likely single, but highly mobile peptide conformation in this subtype.

Influence of temperature on the pVIPR conformations

This inconsistency between the NMR data, measured at 310 K and the X-ray crystallographic results obtained previously at 100 K prompted us to crystallize and analyze the pVIPR-B*27:05 complex at room temperature (RT) to exclude a possible artifact due to the cryogenic temperature. The crystal structure of the pVIPR-B*27:05 complex (see Table 1 for data collection and refinement statistics) unambiguously reveals that pVIPR does not adopt the expected dual peptide-binding mode, as described by us before (9). Instead, at RT, the peptide is displayed by B*27:05 only in the NC conformation. This is in agreement with the lack of double signals in the recorded NMR spectra but not in line with the crystallographic data obtained previously. To resolve this discrepancy, we re-investigated the peptide binding mode at cryogenic temperature (Table 1) and were able to confirm the single NC conformation as observed at RT (Fig. 2*A*). Apart from an alteration of the side chain conformation of pLys-3 and an increased number of defined water molecules at 100 K, both structures are indistinguishable by conventional refinement procedures. Comparable analyses of pVIPR-B*27:09 showed that, irrespective of the temperature, the peptide is retained in the CC conformation, in agreement with our previously published results (9).

*Origin of the dual pVIPR conformation in B*27:05*

Intrigued by the origin of the dual peptide-binding mode described previously, we performed a detailed comparison of the crystal structures. This revealed that in the formerly obtained complexes of both subtypes, a metal ion was bound to pHis-8 that is missing in the *de novo* determined structures, suggesting that this metal ion might have induced the dual peptide conformation. We had previously considered this possibility but had rejected it, because the pVIPR-B*27:09 complex had been found to display the metal ion binding to pHis-8 as well.

A potential influence of metal ions on pVIPR conformations was investigated again after an initial selection, taking the possible coordination of metal ions by histidine residues into account. We were guided by the principle of "hard and soft

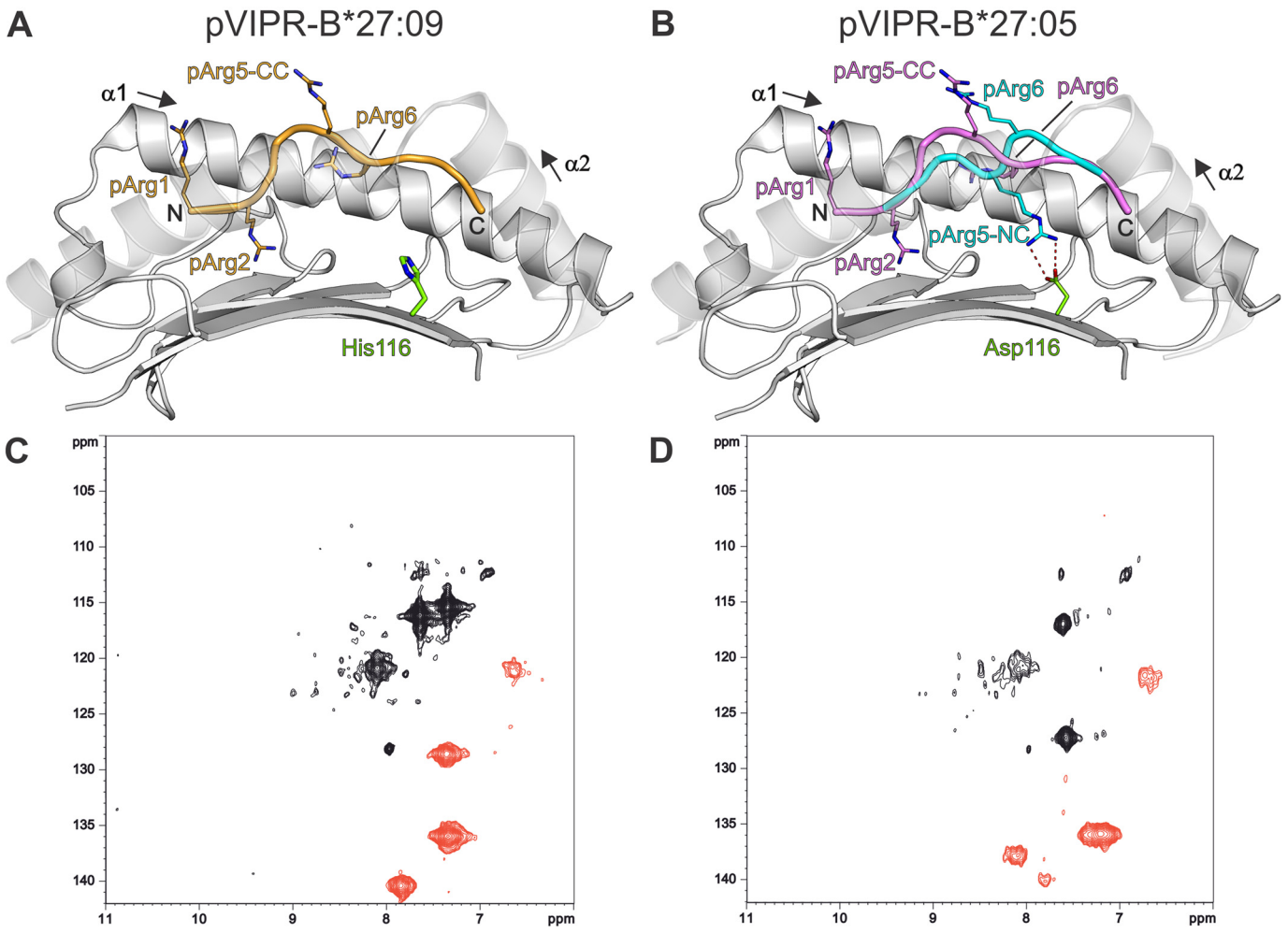

Figure 1. Peptide binding to HLA-B*27 subtypes. According to previously published work (9), the pVIPR peptide binds to the B*27:09 subtype in the CC conformation shown in *orange*. The view is through the α2-helix onto the α1-helix. The peptide is drawn as a *ribbon* and arginine residues in *stick representation* (*A*), whereas a dual binding mode (CC/NC) was observed for B*27:05. The CC conformation is shown in *magenta*, and the NC conformation is in *cyan* (*B*), where pArg-5 forms a salt bridge (*red dashed lines*) to HC residue Asp-116 in the NC-binding mode. This contact is precluded in B*27:09 (His-116) due to electrostatic repulsion. SOFAST-^{1}H,^{15}N-HMQC spectra of both pVIPR-HLA-B*27 complexes containing ^{15}N,^{13}C-labeled Arg at positions 1, 2, 5, and 6 of the peptide are shown in B*27:09 (*C*) and B*27:05 (*D*); the appearance of natural abundance signals from the HC and β_2m in the center of the spectra is due to the long experiment duration. Despite the broad lines, the spectrum for B*27:09-complexed pVIPR appears as expected, with three backbone peaks for pArg-2, pArg-5, and pArg-6 (*black*) and four peaks for the side chains of the four Arg residues mentioned above (*red*). In the spectrum of pVIPR-B*27:05, however, only two peaks for backbone resonances are visible (*black*) instead of the expected five; in addition, only four peaks for the side chains of Arg residues (*red*) can be observed (six are expected).

acids and bases" (18, 19) and the occurrence of metal ions in proteins (20–22). This led us to choose Cu^{2+}, Ni^{2+}, Mn^{2+}, Zn^{2+}, and Hg^{2+} for experiments with crystals of pVIPR-B*27:05 and pVIPR-B*27:09.

We soaked crystals with these metal ions and determined the crystal structures of all metal-treated complexes at 100 K to atomic resolution (see "Experimental procedures"; Fig. 2, *B* and *C*). Table 1 provides the X-ray data collection and refinement statistics. In addition, to precisely identify the respective metal-binding sites in the complexes, we collected the diffraction data at longer wavelengths to record the anomalous signal of the metal ions. These analyses show that the overall architecture of all complexes is not altered by the treatment with metal ions and that structural investigation of the crystals of pVIPR-B*27:05 and pVIPR-B*27:09 soaked with Mn^{2+}, Zn^{2+}, or Hg^{2+} does not reveal any bound metal ion. However, soaking with Cu^{2+} or Ni^{2+} shows that the B*27:05 complex exhibits two metal-binding sites, the first being part of the peptide, where the side chain of pHis-8 is contacted, and the second located outside of the peptide binding groove, near the N terminus of the HC (Fig. 2*B*). In B*27:09, we observed a third Cu^{2+}-binding site in the α3 domain of the HC (Fig. 2*C*).

Because the newly solved structure of pVIPR-B*27:09 possesses a different unit cell than the previously determined structure of this subtype (9), we re-investigated the latter structure (PDB code 1OF2) (9) in terms of metal-binding sites. As in B*27:05, two metal ions are indeed present as well. The first, contacting pHis-8, had tentatively been interpreted as Mn^{2+}, whereas the second binding site at the N terminus of the HC had previously been overlooked. Consequently, together with the newly obtained results, there are two nonisomorphous data sets of the pVIPR-B*27:09 subtype with two identical metal-binding sites. In contrast, the data sets of the metal-soaked pVIPR-B*27:05 crystals and the previously published structure of this complex (PDB code 1OGT) (9) are isomorphous. It is thus possible to rule out any influence

Table 1
Data collection and refinement statistics

	B*27:05-RT	B*27:05–100 K	B*27:05-Cu^{2+}	B*27:05-Ni^{2+}	B*27:09-Cu^{2+}
Data collection					
PDB entry	5IB1	5IB2	5IB3	5IB4	5IB5
Synchrotron source	BESSY II	BESSY II	PETRA III	BESSY II	BESSY II
Temperature	295 K	100 K	100 K	100 K	100 K
Space group	$P2_1$	$P2_1$	$P2_1$	$P2_1$	$P2_1$
Wavelength (Å)	0.9184	0.9184	1.1266	1.1270	0.9184
Unit cell *a*; *b*; *c* (Å)	51.5; 83.1; 66.5	51.2; 82.1; 66.1	51.3; 82.1; 65.4	51.1; 81.7; 65.1	51.0; 81.7; 126.5
α; β; γ (degrees)	90.0; 109.4; 90.0	90.0; 109.5.; 90.0	90.0; 107.6; 90.0	90.0; 107.8; 90.0	90.0; 96.7; 90.0
Resolution (Å)[a]	30.00–1.91 (1.96–1.91)	50.00–1.44 (1.53–1.44)	35.00–1.91 (2.02–1.91)	35.00–1.95 (2.00–1.95)	43.00–2.49 (2.64–2.49)
Unique reflections[a]	40,810 (2817)	92,249 (14,641)	71,965 (9939)	69,349 (3549)	66,171 (2357)
Completeness[a]	99.2 (93.4)	98.8 (97.3)	90.9 (77.6)	94.6 (65.6)	92.9 (89.6)
$\langle I/\sigma(I)\rangle$[a]	12.92 (1.70)	27.51 (5.45)	15.33 (3.61)	14.76 (6.43)	8.30 (2.42)
R_{meas}[a,b]	0.082 (0.751)	0.047 (0.420)	0.046 (0.233)	0.118 (0.310)	0.090 (0.294)
$CC_{½}$[a]	99.8 (64.2)	99.9 (92.3)	99.8 (94.3)	99.5 (65.6)	99.3 (91.9)
Redundancy[a]	3.3 (2.8)	6.9 (6.4)	1.6 (1.4)	3.6 (1.4)	1.2 (1.2)
Wilson *B*-factor (Å^2)	32.4	20.9	27.4	31.1	32.7
Refinement					
Resolution[a]	29.37–1.91 (1.98–1.91)	29.30–1.44 (1.49–1.44)	35.00–1.91 (1.93–1.91)	34.10–1.95 (1.98–1.95)	43.00–2.49 (2.52–2.49)
Non-hydrogen atoms	3375	3747	3638	3555	6634
R_{work}[a,c]	0.166 (0.260)	0.137 (0.148)	0.170 (0.271)	0.164 (0.164)	0.214 (0.300)
R_{free}[a,d]	0.191 (0.301)	0.161 (0.193)	0.204 (0.293)	0.202 (0.223)	0.272 (0.384)
Average *B*-factor (Å^2)	30.5	20.5	29.1	33.6	35.4
HC residues	276/29.0	276/18.0	276/27.4	276/33.3	552/34.9
β_2m residues	100/35.3	99/22.4	100/34.1	100/35.9	200/38.3
pVIPR residues	9/24.3	9/15.2	9/21.9	9/22.7	18/27.8
Metal ion			2/43.1	2/31.9	6/71.3
Buffer molecules		4/36.2	2/39.5	2/40.4	2/29.4
Water molecules	136/31.0	433/30.4	268/31.6	195/33.8	195/30.1
RMSD[e]					
Bond length (Å)	0.007	0.008	0.015	0.016	0.007
Bond angles (degrees)	1.071	1.011	1.313	1.298	0.988
Ramachandran outliers (%)	0.26	0.25	0.25	0.00	0.13
Ramachandran allowed (%)	98.2	98.7	97.3	97.2	96.1

[a] Values in parentheses refer to the highest-resolution shell.
[b] $R_{meas} = \Sigma h(n/(n-1))1/2\Sigma i|Ih - Ih,i|/\Sigma h\Sigma i\, Ih,i$, where *Ih* is the mean intensity of symmetry-equivalent reflections and *n* is the redundancy.
[c] $R_{work} = \Sigma h|F_o - F_c|/\Sigma F_o$ (working set, no σ cut-off applied).
[d] R_{free} is the same as R_{cryst}, but calculated on 5% of the data excluded from refinement.
[e] Root mean square deviation from target geometries.

of a neighboring HC within the crystal lattice on the peptide-binding mode.

This allows us to conclude that, apart from the polymorphic residue 116 and the subtype-specific peptide-binding mode, the pVIPR-B*27:09 complex is a precise structural image of pVIPR-B*27:05, with one remarkable exception: the binding of Cu^{2+} or Ni^{2+} induces a partial conformational reorientation of pVIPR (residues pLys-3 to pTrp-7) only in B*27:05 (Fig. 2, compare *B* and *C*), in which roughly 60% of the peptide is presented in the CC-binding mode and the remaining 40% in the original NC conformation. It seems likely that the simultaneous presence of two pVIPR conformations upon metal ion contact is due to the existence of energetically roughly equally favored peptide-binding modes in which the CC conformation in pVIPR-B*27:05 requires the presence of the inorganic ligand. The contact to His-197 of a neighboring HLA class I molecule (Fig. 3, *A* and *B*) is almost certainly no option outside of a crystal lattice, so that a metal ion would probably have to be coordinated not only by pHis-8, but in addition by further suitable residues from other proteins to be stabilized. An example of how this could be accomplished is provided by an HLA-DR molecule and an interacting T cell receptor (TCR) whose residues jointly contact a Ni^{2+} cation (23).

Because identical treatments of the pVIPR-complexed B*27:05 and B*27:09 subtypes with selected metal ions lead to clearly distinguishable structures, we can rule out that crystallographic artifacts are responsible for the observations. Instead, the Asp-116–mediated increased flexibility of the B*27:05 subtype (11–14) appears as a prerequisite for the peptide conformations reported here (Fig. 1*D*). Only in the case of the AS-associated subtype will the addition of Ni^{2+} or Cu^{2+} favor the acquisition of a dual peptide-binding mode.

Analysis of pVIPR dynamics by ensemble refinement

The results described above not only demonstrate that certain metals can influence the conformation of a displayed peptide, but also indicate that the dynamic behavior of pVIPR is less pronounced when bound to B*27:09 (Fig. 1*C*) than to B*27:05 (Fig. 1*D*). We sought to investigate this further by using ensemble refinements of three complexes presenting pVIPR, all at 100 K: 1) B*27:05 without bound metal ion, 2) B*27:09 with bound Cu^{2+}, and 3) B*27:05 with bound Cu^{2+} in CC- or in NC-binding mode. As expected from NMR spectroscopy (Fig. 1, *C* and *D*), the dynamic differences between B*27:05- and B*27:09-bound pVIPR are pronounced (Fig. 4). Whereas the primary anchor pArg-2 displays only negligible mobility in both subtypes, all other peptide residues show striking plasticity in the B*27:05 complex (peptide in NC-binding mode), in particular pLys-3, pTrp-4, pArg-5, pArg-6, and pHis-8. In B*27:09 (peptide in CC binding mode), only the solvent-exposed pArg-5 exhibits a moderate degree of plasticity. Although the solvent-accessible pArg-1 side chain is mobile in both subtypes, the

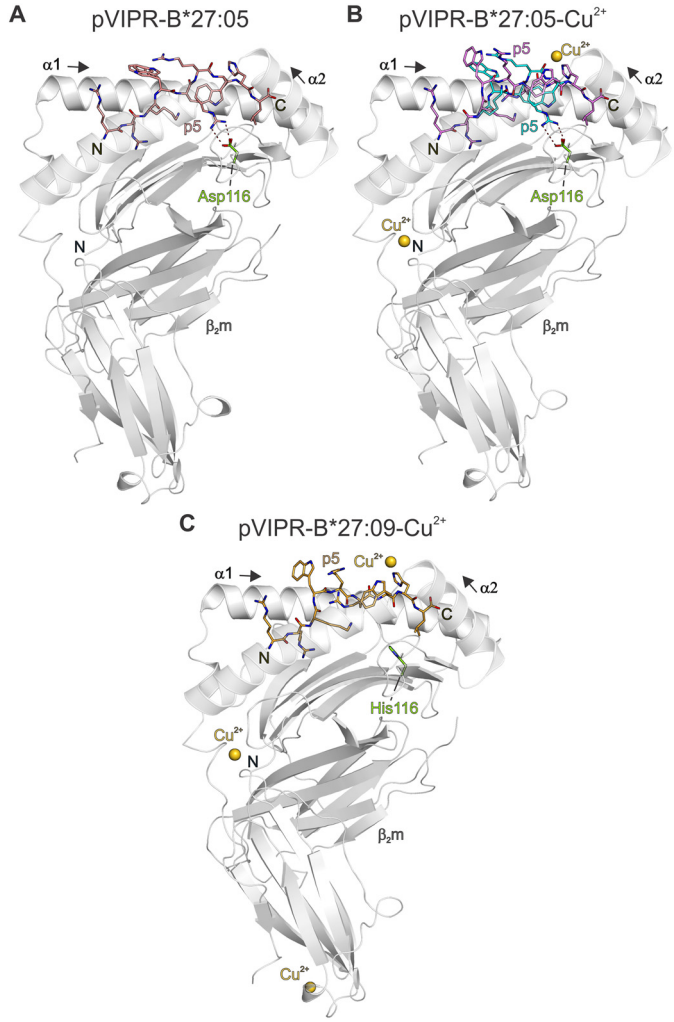

Figure 2. pVIPR conformations and metal binding sites. HLA-B*27 complexes are shown in *gray cartoon* and the respective peptide in *stick representation*; the polymorphic residue at position 116 at the floor of the peptide binding groove is drawn in *green*, and the view is through the α2-helix onto the α1-helix. *A*, in the 100 K as well as in the RT structure, B*27:05 displays the peptide (*pink*) exclusively in the NC conformation. The NC binding mode allows the establishment of a salt bridge (*red dashed lines*) between pArg-5 and the HC residue Asp-116. *B*, a dual peptide-binding mode (*CC/NC*; same *color coding* as in Fig. 1*A*) is induced by Cu^{2+} or Ni^{2+} ions bound to B*27:05. The Cu^{2+} cations are depicted as *yellow spheres*. *C*, in contrast, B*27:09 displays pVIPR in the CC-binding mode, irrespective of the presence or absence of metal ions. The HC residue His-116 precludes a direct contact with pArg-5 of the peptide.

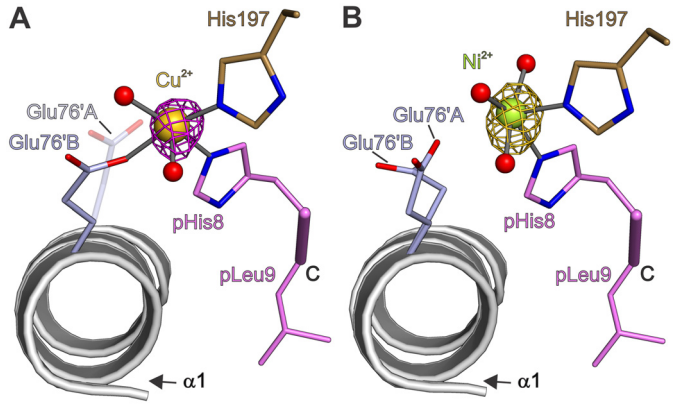

Figure 3. Coordination of Cu^{2+} and Ni^{2+} bound to pVIPR-HLA-B*27 complexes. A given cation is coordinated identically when bound to pVIPR complexes of the two subtypes, but there are differences in coordination between the two metal ions. Anomalous difference maps are contoured at 8 σ in *all panels* around the respective metal ion. *A*, view along the α1-helix toward the C terminus of the peptide. Only the two C-terminal peptide residues (pHis-8, pLeu-9) are shown (*violet*). The coordination of Cu^{2+} in B*27:05 depicts the involvement of pHis-8. Further coordinating residues are Glu-76 (side chain conformation B), two water molecules shown as *red spheres*, and His-197 from a neighboring HLA-B*27 molecule. *B*, the coordination of Ni^{2+} in B*27:05 is shown. Instead of Glu-76, an additional water molecule contributes to coordinate the cation.

ensemble of structures that is revealed by the improved type of refinement is larger in B*27:05 than in B*27:09.

Furthermore, a comparison of pVIPR dynamics in the NC- and CC-binding modes to B*27:05 was carried out (Fig. 5). This analysis reveals that pVIPR retains its overall plasticity irrespective of the peptide-binding mode, but pLys-3 and pArg-5 exhibit a diminished degree of conformational dynamics in the NC conformation. The most conspicuous difference following the binding of Cu^{2+} concerns pHis-8 and pLeu-9; in both cases (Fig. 5), the side chains show very little mobility compared with the metal-free state (Fig. 4, *A* and *B*).

Finally, the metal ion-induced CC conformation of the peptide in B*27:05 exhibits a much higher extent of flexibility of nearly all amino acid side chains when compared with the CC-binding mode of pVIPR to B*27:09 (Figs. 4 (*B and D*) and 5 (*B* and *D*)). This elevated plasticity even encompasses the pArg-1 side chain, at a distance of ~20 Å from the polymorphic HC residue Asp/His-116.

On the number of self-peptides permitting a dual binding mode

Using a data bank search, we also addressed the question of how many self-peptides could be identified that would allow metal ions to bind in a manner comparable with that observed here for pVIPR-B*27:05, thereby possibly leading to dual peptide presentation modes by B*27:05 molecules. In this way, a distinct "arthritogenic" peptide (24), currently still an elusive entity, might not be needed as triggering agent for the development of AS. This data bank search (see "Experimental procedures") revealed that 823 human proteins could act as donors for 873 nonamer self-peptides that might be displayed by the B*27:05 subtype, appear potentially able to bind metal ions, and could be subject to conformational reorientation. Because B*27:05 exhibits no absolute requirement for pArg-2 of a bound peptide (25), the number of such self-peptides might be even larger. Interestingly, none of the 26 candidate peptides identified by Schittenhelm and colleagues (26, 27) as potentially arthritogenic fulfills the requirements outlined above.

Discussion

Our study reveals three principal experimental findings: 1) the pVIPR peptide is normally presented in a single (NC) conformation by B*27:05, not in a dual (NC+CC) binding mode as published previously by us (9); 2) the binding of selected metal ions to pHis-8 leads to the acquisition of a dual (NC+CC) conformation of pVIPR, but only in the AS-associated B*27:05 subtype; 3) both NMR spectroscopy and ensemble refinements of crystallographic structures show that pVIPR exhibits a different

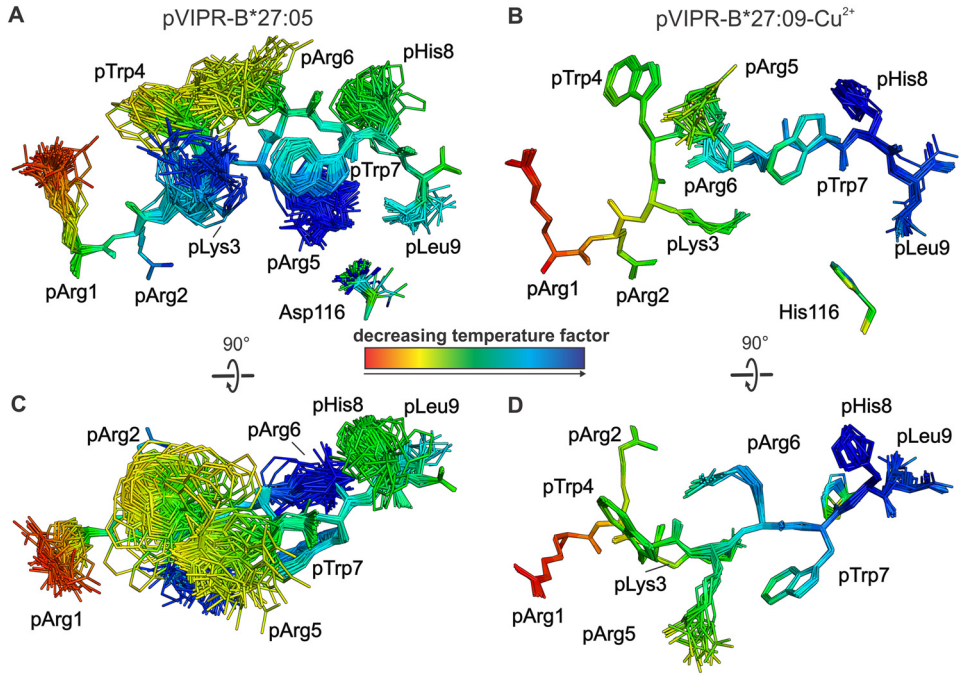

Figure 4. Results of the ensemble refinement performed for the structures of pVIPR bound to B*27:05 and B*27:09, respectively. For clarity, the HC and β_2m are not shown. The peptide and the polymorphic residue at position 116 are displayed in a *stick representation*. The peptide is *color-coded* by decreasing temperature factor from *red* to *blue*. *A*, pVIPR-B*27:05 shows increased dynamics; *B*, pVIPR shows a lower degree of flexibility when presented by B*27:09. *C*, view of *A* rotated by 90°. pVIPR-B*27:05 is oriented such that an approaching TCR would "see" the peptide. *D*, view of *B* rotated by 90°. pVIPR-B*27:09 is oriented such that an approaching TCR would "see" the peptide.

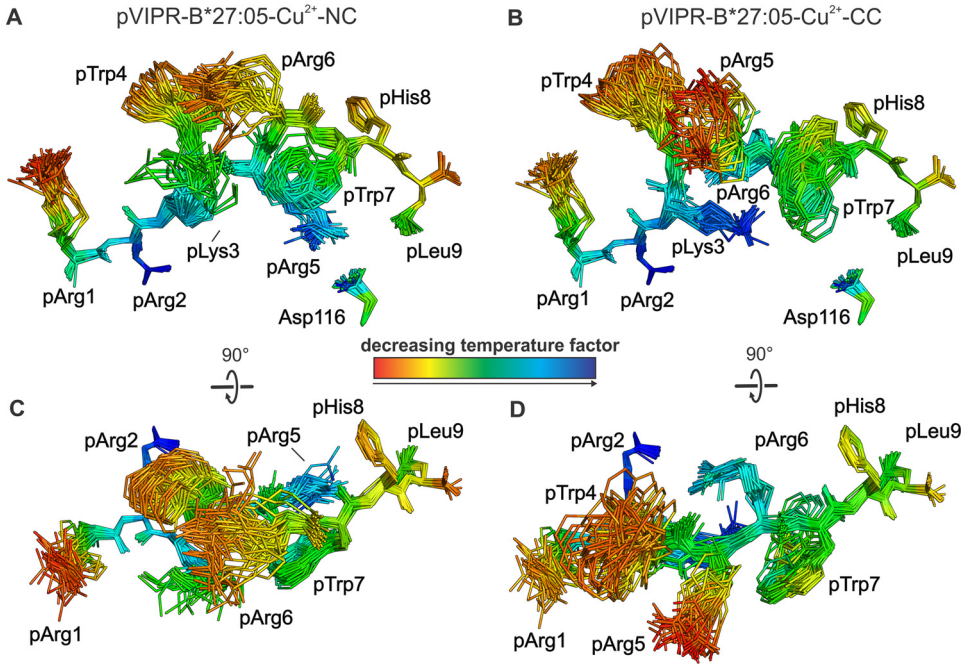

Figure 5. Results of the ensemble refinement performed for the structures of pVIPR bound to B*27:05 in the presence of Cu^{2+}. For clarity, the HC and β_2m are not shown. The peptide and the polymorphic residue at position 116 are displayed in a *stick representation*. The peptide is *color-coded* by decreasing temperature factor from *red* to *blue*. *A*, pVIPR-B*27:05-Cu^{2+} in NC conformation; *B*, pVIPR-B*27:05-Cu^{2+} in the CC conformation. *C*, view of *A* rotated by 90°, such that an approaching TCR would "see" the peptide. *D*, view of *B* rotated by 90°, such that an approaching TCR would "see" the peptide.

dynamics when bound to B*27:05, as compared with B*27:09, where it is less mobile than in B*27:05.

The structure of an MHC class I molecule can thus be affected in an allele-specific fashion by certain metal ions that bind to an exposed histidine residue of a displayed peptide, leading to a gross structural reorientation of the ligand, but only in the B*27:05 subtype. Cu^{2+} and Ni^{2+} are known to bind to histidine side chains (20–22), and it is conceivable that the mobility of pHis-8 is reduced (compare Figs. 4*A* and 5*A*) due to metal binding. In what way the dynamics of several further peptide residues is influenced, however, remains currently a matter of speculation. Changes involving the protonation of His resi-

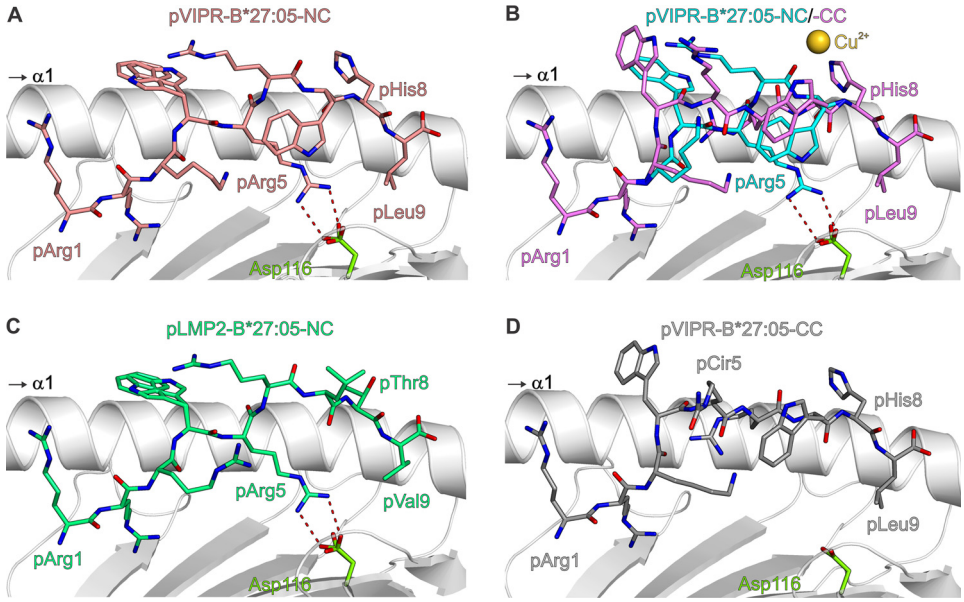

Figure 6. Differential presentation of pVIPR and closely related ligands by the B*27:05 subtype. All B*27:05-bound ligands are shown in identical orientation, through the α2-helix (removed) onto the α1-helix (*gray*). *A*, pVIPR bound in the NC conformation. Note the establishment of a salt bridge between pArg-5 and the HC residue Asp-116, indicated by *red dashed lines*. *B*, pVIPR bound in a dual conformation (NC in *cyan*, CC in *magenta*) triggered by a Cu^{2+} ion in the vicinity of pHis-8. *C*, pLMP2 bound in the NC conformation. Note the molecular mimicry between this structure and that of pVIPR shown in Fig. 3*A*. *D*, pVIPR with pArg-5 replaced by citrulline. This neo-antigen is bound in the CC conformation, closely resembling that found for pVIPR-CC (*B*), because a contact between the side chain of citrulline and Asp-116 cannot be established.

dues have already been described for HLA-DR molecules (28) as well as for pVIPR-B*27:09, where a decreased stability of the complex was detected when the pH of the medium was reduced from 7.5 to 5.6 (13). In addition, using fluorescence depolarization and pK_a calculations, we have previously described an allosteric interaction between pHis-8 and the HC Glu-45/63 pair of residues, which contribute to anchoring pArg-2 within the B pocket of the binding groove (29). Comparable long-range interactions have also been identified for HC residue 116 with β_2m (30) or through β_2m to the most distal region of the α3 domain (31). NMR spectroscopic analyses of the B*27:05 and B*27:09 HC might shed new light on the reasons for the far-reaching effects of conformational changes affecting pHis-8.[5]

The novel insight into the acquisition of the NC- and CC-pVIPR binding modes explains functional data (9, 10) showing the existence of CTL from B*27:05-positive individuals that react with this peptide in the context of both subtypes; it seems very likely that it is the CC conformation that forms the basis for recognition by these CTL, because CTL are expected to be negatively selected in the thymus on B*27:05-positive cells displaying NC-pVIPR. Only a single CTL from a *B*27:05*-positive donor was found that reacted with B*27:05 but not B*27:09, in line with an NC-pVIPR–specific reactivity (9).

The two conformations of pVIPR in B*27:05 resemble also those found for the viral pLMP2 peptide (RRRWRRLTV, derived from Epstein–Barr virus latent membrane protein 2 (PDB code 1UXS (32)) (Fig. 6*C*) and for the citrullinated pVIPR (PDB 3B6S) (33) (Fig. 6*D*), in the same subtype, respectively. In the former case, pLMP2 is displayed solely in the NC conformation (32), whereas citrullinated pVIPR is presented exclusively in the CC-binding mode due to the loss of the positively charged guanidinium group of pArg-5 through the replacement of this peptide residue by citrulline (33). The various peptide-binding modes that we describe here for the B*27:05 subtype could be regarded as an example of how structural differences between self-ligands (Fig. 6*A*), altered self-peptides (also termed neo-antigens) (Fig. 6, *B* and *D*), and closely related foreign antigens (Fig. 6*C*) presented by MHC class I molecules can be blurred (34). The higher degree of flexibility, which characterizes the B*27:05 binding groove, in contrast to that of B*27:09 (11–14), forms the basis for the differential, Asp/His-116 – dependent display of similar ligands.

In line with a recent ensemble refinement study of several MHC-bound peptides by Fodor *et al.* (35), our work demonstrates also that the extent of peptide dynamics has been underestimated using conventional X-ray crystallography refinement alone. The results from our NMR spectroscopic experiments and the dynamics-oriented refinements support each other (Figs. 1 (*C* and *D*) and 4 (*A* and *B*)). They show that ensemble refinement techniques will greatly improve our understanding of the conformational plasticity of peptides presented by MHC molecules and shed new light on their interactions with TCR and other extracellular ligands.

However, plasticity of HC residue 116 and the peptide terminus-binding F pocket in general (see also the subtypes B*44:02 and B*44:05 (36)) is not only crucial for permitting appropriate T-cell responses but affects also interactions with intracellular ligands, most prominently tapasin (37, 38) and TAP-binding protein (TAPBPR) (39–41). The great variety of molecular contacts has recently been reviewed (42). Virtually all of these interactions critically rely on dynamics of the binding partners. Due to the experimental difficulties accompanying NMR spectros-

[5] M. Ballaschk, B. Loll, A. Ziegler, B. Uchanska-Ziegler, and P. Schmieder, manuscript in preparation.

copy, we expect that extracting dynamic information from existing X-ray diffraction data sets by ensemble refinements (16, 35) will be very helpful in providing further insight into the conformational flexibility of MHC molecules and their protein ligands.

The results presented here not only illuminate the dynamics of HLA class I molecules but also allow us to draw some conclusions regarding the involvement of metal ions in disease. Although such ions perform essential functions in physiological processes, as in enzyme catalysis, signal transduction, and electron transfer, many are also known to cause grave health problems in humans, leading to hypersensitivities and allergies in more than 10% of the world's population (43). There are several ways by which metals could initiate inappropriate T cell responses (44). Here we describe one possibility, the conformational reorientation of a bound peptide, induced by its interaction with Cu^{2+} or Ni^{2+}. Another mechanism is observed in patients with chronic beryllium disease (45), where Be^{2+} is coordinated by residues of an HLA class II molecule (HLA-DP2) forming an acidic pocket within the binding groove. The metal ion contributes to the selection of peptides that share pAsp-4 and pGlu-7, apparently to improve the stability of the assembly by interacting with the metal ion. A TCR has no opportunity to recognize the bound Be^{2+} ion but is indirectly affected by conformational changes of the HLA-DP2 molecule's surface and its altered electrostatic potential (34). Much less is known, however, about the molecular basis for nickel-induced contact hypersensitivities, although this metal is the most common occupational and public contact allergen (43). There is evidence that Ni^{2+} ions can interact with an HLA-DR–bound peptide (46), with an HLA-DR molecule and a bound peptide (47), as well as jointly with an HLA-DR molecule and a TCR (23), but there are no structural data to support any of these findings.

As we show here, metals can influence antigen presentation also in the case of an MHC class I molecule and are therefore potential triggering agents for disease development due to their omnipresence. An example of the role that metals can play in setting off spondyloarthropathies is provided by Brown Norway rats, whose relative genetic resistance to *Chlamydia*-induced reactive arthritis (an *HLA-B*27*-associated disease in humans) can be overcome by injections of mercuric chloride, leading to a marked exacerbation of the severity of arthritic symptoms in the animals (48). Explanatory difficulties connected with the fact that only certain *HLA* alleles are associated with a particular disease could be accounted for by assuming that conformational reorientations of a peptide as described here for the pVIPR-B*27:05 complex following exposure to Cu^{2+} or Ni^{2+} are less likely in subtypes that lack a disease association, such as *B*27:09*. As mentioned before, a particular arthritogenic peptide (24), possibly derived from a microorganism, would be superfluous in this scenario. A higher degree of molecular dynamics in the AS-associated subtypes B*27:05 and B*27:04 than in the nonassociated B*27:09 and B*27:06 molecules (15) supports the idea that HLA-B*27 polymorphisms, molecular flexibility, concomitant peculiarities in peptide repertoire, and presentation and ultimately AS association are intimately connected with each other.

Furthermore, the so far unexplained fact that smoking contributes to a more severe course of AS (49–51) and other diseases, including rheumatoid arthritis (49, 50), is also of interest in the context described here, because tobacco smoke contains not only toxic organic compounds, but also several metals, including nickel (52). In individuals with *HLA* class I or II alleles predisposing to rheumatic disorders, prophylactic measures can thus be suggested, including the avoidance of tobacco abuse and environmental tobacco smoke exposure as well as minimizing the contact with metals known to cause allergies. Our results might even provide the rationale for a therapeutic intervention, such as a treatment with chelating agents (53). For AS, *HLA-B*27:05*/human β_2m-transgenic rats developing AS-like symptoms (54) would be suitable to test several of these assumptions.

It remains to be determined, however, whether conformational reorientations of peptides bound to class I antigens other than HLA-B*27 can provide the basis for neo-antigen creation in further cases of metal-induced hypersensitivities and allergies (55–57) and whether hypersensitivities and autoimmunity do really represent two sides of the same coin (45, 58).

Experimental procedures

NMR spectroscopy

Samples of the complexes were produced as described previously (30) and contained 17.6 mg/ml pVIPR-B*27:09 and 10.1 mg/ml pVIPR-B*27:05, respectively, with the peptide synthesized at the Core Facility of the University of Leipzig (Germany) using conventional Fmoc-peptide synthesis utilizing ^{15}N,^{13}C-labeled arginine. The buffer used for NMR spectroscopy contained 150 mM NaCl and 10 mM sodium phosphate, pH 7.5. NMR spectra were recorded as SOFAST-^{1}H,^{15}N-HMQC (59) at 310 K in a buffer free from Cu^{2+}, Hg^{2+}, Mn^{2+}, Ni^{2+}, and Zn^{2+} on an AV750 Bruker spectrometer (750 MHz ^{1}H frequency) with identical parameters: 4000 scans, data size 512(^{1}H)*64(^{15}N) complex points, t_{Hmax} = 440.8 ms, t_{Nmax} = 16.8 ms. A recycle delay of 0.1 s was used, resulting in an experiment duration of 20 h.

Crystallography

For crystallization experiments, the pVIPR-B*27:09 and pVIPR-B*27:05 proteins were prepared as described before (9). One protein preparation from a given subtype was used for all crystallization and soaking experiments. Crystallization trials and cryoprotection were performed according to the protocol described previously (9). Soaking experiments were carried out at a concentration of 50 mM for the chloride salt of the respective metal ion for 2 min. For measurements at RT, the crystals were mounted in MicroRT™ capillaries (MiTeGen, Ithaca, NY). X-ray diffraction data sets were collected at beamline 14.2 of the MX Joint Berlin laboratory at the BESSY II in Berlin, Germany, or at the beamline P14 at PETRA III in Hamburg, Germany. Anomalous diffraction data were collected at the wavelength as indicated in Table 1. Diffraction data were processed with the XDS package (60). Data collection and refine-

ment statistics are given in Table 1. The following complexes with pVIPR were analyzed by X-ray crystallography: B*27:05 at room temperature, B*27:05 at 100 K, B*27:05 at 100 K soaked with Cu^{2+}, Ni^{2+}, Mn^{2+}, Zn^{2+}, or Hg^{2+}; B*27:09 at room temperature, B*27:09 at 100 K soaked with Cu^{2+}, Ni^{2+}, Mn^{2+}, Zn^{2+}, or Hg^{2+}. Atomic coordinates and structure factor amplitudes were deposited in the Protein Data Bank under accession codes 5IB1 (pVIPR-B*27:05 at RT), 5IB2 (pVIPR-B*27:05 at 100 K), 5IB3 (pVIPR-B*27:05 Cu^{2+}-soaked), 5IB4 (pVIPR-B*27:05 Ni^{2+}-soaked), and 5IB5 (pVIPR-B*27:09 Cu^{2+}-soaked).

Structure determination, refinement, and analysis

The structures were solved by molecular replacement with pVIPR-B*27:05 (PDB code 1OGT (9)) as search model using the program PHASER (61) and refined by annealing and maximum-likelihood restrained refinement in PHENIX (62) followed by iterative model building cycles in COOT (63). Water molecules were positioned with COOT and manually inspected. Intermediate and final structures were evaluated with MOLPROBITY (64). The starting structures for ensemble refinements as implemented in PHENIX (62) were prepared as described (16). Briefly, alternate conformations of amino acid side chains were removed from the deposited structures in the PDB, and the occupancies were adjusted to 1. For the structure pVIPR-B*27:05-Cu^{2+}, all double conformations were removed except those of the pVIPR peptide. The occupancy of each of the two peptide conformations was set to 0.5. Explicit hydrogen atoms were generated with phenix.ready_set. The ensemble refinements were executed with the standard settings except that the scale factor for X-ray/stereochemistry weight (wxc_scale) was adjusted to the value used for standard real-space refinement. For glycerol molecules, harmonic restraints were set to avoid stochastic displacement during simulations. Figures were prepared with PyMOL (65).

Data bank search

SwissProt was accessed on September 15, 2015 to obtain an estimate of the number of human protein–derived nonamer peptides that could principally be presented by B*27:05 and allow metal-induced conformational reorientations. The peptides had to meet the following criteria: no Pro at p1 (Pro is not accepted at this position), pArg-2 (a nearly obligatory anchor for HLA-B*27 molecules (25), no Asp or Glu at p9 (these would not bind with high affinity to B*27:05), and also no Arg or Lys at this position (contact with Asp-116 would preclude the interaction between pArg-5 and Asp-116) (66). As a potential contact site for a metal ion, pHis-8 should also be present as well as a basic residue at p5 to allow binding to HC residue Asp-116 in the NC conformation.

Author contributions—R. D., M. B., P. S., B. U.-Z., A. Z., and B. L. data curation; R. D., M. B., P. S., B. U.-Z., A. Z., and B. L. formal analysis; R. D., M. B., P. S., B. U.-Z., A. Z., and B. L. validation; R. D., M. B., P. S., and B. L. visualization; M. B. investigation; P. S., B. U.-Z., A. Z., and B. L. conceptualization; P. S., B. U.-Z., A. Z., and B. L. supervision; P. S., B. U.-Z., A. Z., and B. L. funding acquisition; P. S., B. U.-Z., A. Z., and B. L. writing-original draft.

Acknowledgments—We are grateful to Christina Schnick and Claudia Alings for excellent technical assistance. We acknowledge access to beamline BL14.2 of the BESSY II storage ring (Berlin, Germany) via the Joint Berlin MX-Laboratory sponsored by the Helmholtz Zentrum Berlin für Materialien und Energie, the Freie Universität Berlin, the Humboldt-Universität zu Berlin, the Max-Delbrück Centrum, and the Leibniz-Institut für Molekulare Pharmakologie. We also acknowledge beamtime and support at beamline P14 of PETRA III (Deutsches Elektronen Synchrotron, Hamburg, Germany).

References

1. Schlosstein, L., Terasaki, P. I., Bluestone, R., and Pearson, C. M. (1973) High association of an HL-A antigen, W27, with ankylosing spondylitis. *N. Engl. J. Med.* **288,** 704–706 CrossRef Medline
2. Brewerton, D. A., Hart, F. D., Nicholls, A., Caffrey, M., James, D. C., and Sturrock, R. D. (1973) Ankylosing spondylitis and HL-A 27. *Lancet* **1,** 904–907 CrossRef Medline
3. Bowness, P. (2015) HLA-B27. *Annu. Rev. Immunol.* **33,** 29–48 CrossRef Medline
4. Colbert, R. A., Navid, F., and Gill, T. (2017) The role of HLA-B*27 in spondyloarthritis. *Best Pract. Res. Clin. Rheumatol.* **31,** 797–815 CrossRef Medline
5. López de Castro, J. A. (2018) How ERAP1 and ERAP2 shape the peptidomes of disease-associated MHC-I proteins. *Front. Immunol.* **9,** 2463 CrossRef Medline
6. McGonagle, D., Aydin, S. Z., Gül, A., Mahr, A., and Direskeneli, H. (2015) 'MHC-I-opathy'-unified concept for spondyloarthritis and Behcet disease. *Nat. Rev. Rheumatol.* **11,** 731–740 CrossRef Medline
7. Uchanska-Ziegler, B., Loll, B., Fabian, H., Hee, C. S., Saenger, W., and Ziegler, A. (2012) HLA class I-associated diseases with a suspected autoimmune etiology: HLA-B27 subtypes as a model system. *Eur. J. Cell Biol.* **91,** 274–286 CrossRef Medline
8. Fiorillo, M. T., Paladini, F., Tedeschi, V., and Sorrentino, R. (2017) HLA class I or class II and disease association: catch the difference if you can. *Front. Immunol.* **8,** 1475 CrossRef Medline
9. Hülsmeyer, M., Fiorillo, M. T., Bettosini, F., Sorrentino, R., Saenger, W., Ziegler, A., and Uchanska-Ziegler, B. (2004) Dual, HLA-B27 subtype-dependent conformation of a self-peptide. *J. Exp. Med.* **199,** 271–281 CrossRef Medline
10. Fiorillo, M. T., Maragno, M., Butler, R., Dupuis, M. L., and Sorrentino, R. (2000) $CD8^+$ T-cell autoreactivity to an HLA-B27-restricted self-epitope correlates with ankylosing spondylitis. *J. Clin. Invest.* **106,** 47–53 CrossRef Medline
11. Fabian, H., Huser, H., Loll, B., Ziegler, A., Naumann, D., and Uchanska-Ziegler, B. (2010) HLA-B27 heavy chains distinguished by a micropolymorphism exhibit differential flexibility. *Arthritis Rheum.* **62,** 978–987 CrossRef Medline
12. Fabian, H., Huser, H., Narzi, D., Misselwitz, R., Loll, B., Ziegler, A., Böckmann, R. A., Uchanska-Ziegler, B., and Naumann, D. (2008) HLA-B27 subtypes differentially associated with disease exhibit conformational differences in solution. *J. Mol. Biol.* **376,** 798–810 CrossRef Medline
13. Fabian, H., Loll, B., Huser, H., Naumann, D., Uchanska-Ziegler, B., and Ziegler, A. (2011) Influence of inflammation-related changes on conformational characteristics of HLA-B27 subtypes as detected by IR spectroscopy. *FEBS J.* **278,** 1713–1727 CrossRef Medline
14. Narzi, D., Becker, C. M., Fiorillo, M. T., Uchanska-Ziegler, B., Ziegler, A., and Böckmann, R. A. (2012) Dynamical characterization of two differentially disease associated MHC class I proteins in complex with viral and self-peptides. *J. Mol. Biol.* **415,** 429–442 CrossRef Medline
15. Loll, B., Fabian, H., Huser, H., Hee, C. S., Ziegler, A., Uchanska-Ziegler, B., and Ziegler, A. (2016) Increased conformational flexibility of HLA-B*27 subtypes associated with ankylosing spondylitis. *Arthritis Rheumatol.* **68,** 1172–1182 CrossRef Medline

16. Burnley, B. T., Afonine, P. V., Adams, P. D., and Gros, P. (2012) Modelling dynamics in protein crystal structures by ensemble refinement. *Elife* **1,** e00311 CrossRef Medline
17. Gros, P., van Gunsteren, W. F., and Hol, W. G. (1990) Inclusion of thermal motion in crystallographic structures by restrained molecular dynamics. *Science* **249,** 1149–1152 CrossRef Medline
18. Pearson, R. G. (1963) Hard and soft acids and bases. *J. Am. Chem. Soc.* **85,** 3533–3539 CrossRef
19. Pearson, R. G. (1990) Hard and soft acids and bases—the evolution of a chemical concept. *Coordin. Chem. Rev.* **100,** 403–425 CrossRef
20. Harding, M. M. (1999) The geometry of metal-ligand interactions relevant to proteins. *Acta Crystallogr. D Biol. Crystallogr.* **55,** 1432–1443 CrossRef Medline
21. Harding, M. M. (2001) Geometry of metal-ligand interactions in proteins. *Acta Crystallogr.* **57,** 401–411 CrossRef Medline
22. Zheng, H., Cooper, D. R., Porebski, P. J., Shabalin, I. G., Handing, K. B., and Minor, W. (2017) CheckMyMetal: a macromolecular metal-binding validation tool. *Acta Crystallogr. D Struct. Biol.* **73,** 223–233 CrossRef Medline
23. Gamerdinger, K., Moulon, C., Karp, D. R., Van Bergen, J., Koning, F., Wild, D., Pflugfelder, U., and Weltzien, H. U. (2003) A new type of metal recognition by human T cells: contact residues for peptide-independent bridging of T cell receptor and major histocompatibility complex by nickel. *J. Exp. Med.* **197,** 1345–1353 CrossRef Medline
24. Benjamin, R., and Parham, P. (1990) Guilt by association: HLA-B27 and ankylosing spondylitis. *Immunol. Today* **11,** 137–142 CrossRef Medline
25. Ramos, M., Paradela, A., Vazquez, M., Marina, A., Vazquez, J., and Lopez de Castro, J. A. (2002) Differential association of HLA-B*2705 and B*2709 to ankylosing spondylitis correlates with limited peptide subsets but not with altered cell surface stability. *J. Biol. Chem.* **277,** 28749–28756 CrossRef Medline
26. Schittenhelm, R. B., Sivaneswaran, S., Lim Kam Sian, T. C., Croft, N. P., and Purcell, A. W. (2016) Human leukocyte antigen (HLA) B27 allotype-specific binding and candidate arthritogenic peptides revealed through heuristic clustering of data-independent acquisition mass spectrometry (DIA-MS) data. *Mol. Cell Proteomics* **15,** 1867–1876 CrossRef Medline
27. Schittenhelm, R. B., Sian, T. C., Wilmann, P. G., Dudek, N. L., and Purcell, A. W. (2015) Revisiting the arthritogenic peptide theory: quantitative not qualitative changes in the peptide repertoire of HLA-B27 allotypes. *Arthritis Rheumatol.* **67,** 702–713 CrossRef Medline
28. Rötzschke, O., Lau, J. M., Hofstätter, M., Falk, K., and Strominger, J. L. (2002) A pH-sensitive histidine residue as control element for ligand release from HLA-DR molecules. *Proc. Natl. Acad. Sci. U.S.A.* **99,** 16946–16950 CrossRef Medline
29. Narzi, D., Winkler, K., Saidowsky, J., Misselwitz, R., Ziegler, A., Böckmann, R. A., and Alexiev, U. (2008) Molecular determinants of major histocompatibility complex class I complex stability: shaping antigenic features through short and long range electrostatic interactions. *J. Biol. Chem.* **283,** 23093–23103 CrossRef Medline
30. Beerbaum, M., Ballaschk, M., Erdmann, N., Schnick, C., Diehl, A., Uchanska-Ziegler, B., Ziegler, A., and Schmieder, P. (2013) NMR spectroscopy reveals unexpected structural variation at the protein-protein interface in MHC class I molecules. *J. Biomol. NMR* **57,** 167–178 CrossRef Medline
31. Ayres, C. M., Abualrous, E. T., Bailey, A., Abraham, C., Hellman, L. M., Corcelli, S. A., Noé, F., Elliott, T., and Baker, B. M. (2019) Dynamically driven allostery in MHC proteins: peptide-dependent tuning of class I MHC global flexibility. *Front. Immunol.* **10,** 966 CrossRef Medline
32. Fiorillo, M. T., Rückert, C., Hülsmeyer, M., Sorrentino, R., Saenger, W., Ziegler, A., and Uchanska-Ziegler, B. (2005) Allele-dependent similarity between viral and self-peptide presentation by HLA-B27 subtypes. *J. Biol. Chem.* **280,** 2962–2971 CrossRef Medline
33. Beltrami, A., Rossmann, M., Fiorillo, M. T., Paladini, F., Sorrentino, R., Saenger, W., Kumar, P., Ziegler, A., and Uchanska-Ziegler, B. (2008) Citrullination-dependent differential presentation of a self-peptide by HLA-B27 subtypes. *J. Biol. Chem.* **283,** 27189–27199 CrossRef Medline
34. Clayton, G. M., Wang, Y., Crawford, F., Novikov, A., Wimberly, B. T., Kieft, J. S., Falta, M. T., Bowerman, N. A., Marrack, P., Fontenot, A. P., Dai, S., and Kappler, J. W. (2014) Structural basis of chronic beryllium disease: linking allergic hypersensitivity and autoimmunity. *Cell* **158,** 132–142 CrossRef Medline
35. Fodor, J., Riley, B. T., Borg, N. A., and Buckle, A. M. (2018) Previously hidden dynamics at the TCR-peptide-MHC interface revealed. *J. Immunol.* **200,** 4134–4145 CrossRef Medline
36. Zernich, D., Purcell, A. W., Macdonald, W. A., Kjer-Nielsen, L., Ely, L. K., Laham, N., Crockford, T., Mifsud, N. A., Bharadwaj, M., Chang, L., Tait, B. D., Holdsworth, R., Brooks, A. G., Bottomley, S. P., Beddoe, T., Peh, C. A., Rossjohn, J., and McCluskey, J. (2004) Natural HLA class I polymorphism controls the pathway of antigen presentation and susceptibility to viral evasion. *J. Exp. Med.* **200,** 13–24 CrossRef Medline
37. Hafstrand, I., Sayitoglu, E. C., Apavaloaei, A., Josey, B. J., Sun, R., Han, X., Pellegrino, S., Ozkazanc, D., Potens, R., Janssen, L., Nilvebrant, J., Nygren, P. Å., Sandalova, T., Springer, S., Georgoudaki, A. M., Duru, A. D., and Achour, A. (2019) Successive crystal structure snapshots suggest the basis for MHC class I peptide loading and editing by tapasin. *Proc. Natl. Acad. Sci. U.S.A.* **116,** 5055–5060 CrossRef Medline
38. Williams, A. P., Peh, C. A., Purcell, A. W., McCluskey, J., and Elliott, T. (2002) Optimization of the MHC class I peptide cargo is dependent on tapasin. *Immunity* **16,** 509–520 CrossRef Medline
39. Thomas, C., and Tampé, R. (2017) Structure of the TAPBPR-MHC I complex defines the mechanism of peptide loading and editing. *Science* **358,** 1060–1064 CrossRef Medline
40. McShan, A. C., Natarajan, K., Kumirov, V. K., Flores-Solis, D., Jiang, J., Badstübner, M., Toor, J. S., Bagshaw, C. R., Kovrigin, E. L., Margulies, D. H., and Sgourakis, N. G. (2018) Peptide exchange on MHC-I by TAPBPR is driven by a negative allostery release cycle. *Nat. Chem. Biol.* **14,** 811–820 CrossRef Medline
41. Jiang, J., Natarajan, K., Boyd, L. F., Morozov, G. I., Mage, M. G., and Margulies, D. H. (2017) Crystal structure of a TAPBPR-MHC I complex reveals the mechanism of peptide editing in antigen presentation. *Science* **358,** 1064–1068 CrossRef Medline
42. Natarajan, K., Jiang, J., and Margulies, D. H. (2019) Structural aspects of chaperone-mediated peptide loading in the MHC-I antigen presentation pathway. *Crit. Rev. Biochem. Mol. Biol.* **54,** 164–173 CrossRef Medline
43. Wang, Y., and Dai, S. (2013) Structural basis of metal hypersensitivity. *Immunol. Res.* **55,** 83–90 CrossRef Medline
44. Yin, L., Dai, S., Clayton, G., Gao, W., Wang, Y., Kappler, J., and Marrack, P. (2013) Recognition of self and altered self by T cells in autoimmunity and allergy. *Protein Cell* **4,** 8–16 CrossRef Medline
45. Fontenot, A. P., Falta, M. T., Kappler, J. W., Dai, S., and McKee, A. S. (2016) Beryllium-induced hypersensitivity: genetic susceptibility and neoantigen generation. *J. Immunol.* **196,** 22–27 CrossRef Medline
46. Romagnoli, P., Labhardt, A. M., and Sinigaglia, F. (1991) Selective interaction of Ni with an MHC-bound peptide. *EMBO J.* **10,** 1303–1306 CrossRef Medline
47. Lu, L., Vollmer, J., Moulon, C., Weltzien, H. U., Marrack, P., and Kappler, J. (2003) Components of the ligand for a Ni^{++} reactive human T cell clone. *J. Exp. Med.* **197,** 567–574 CrossRef Medline
48. Inman, R. D., and Chiu, B. (2009) Heavy metal exposure reverses genetic resistance to *Chlamydia*-induced arthritis. *Arthritis Res. Ther.* **11,** R19 CrossRef Medline
49. Wendling, D., and Prati, C. (2013) Spondyloarthritis and smoking: towards a new insight into the disease. *Expert Rev. Clin. Immunol.* **9,** 511–516 CrossRef Medline
50. Klareskog, L., Malmström, V., Lundberg, K., Padyukov, L., and Alfredsson, L. (2011) Smoking, citrullination and genetic variability in the immunopathogenesis of rheumatoid arthritis. *Semin. Immunol.* **23,** 92–98 CrossRef Medline
51. Dulger, S., Aykurt Karlibel, I., Kasapoglu Aksoy, M., Altan, L., Sengoren Dikis, O., and Yildiz, T. (2018) How does smoking cessation affect disease activity, function loss, and quality of life in smokers with ankylosing spondylitis? *J. Clin. Rheumatol.* CrossRef Medline
52. Haustein, K.-O., and Groneberg, D. (2008) *Tabakabhängigkeit*, pp. 44–45, Springer-Verlag, Berlin
53. Wax, P. M. (2013) Current use of chelation in American health care. *J. Med. Toxicol.* **9,** 303–307 CrossRef Medline

54. Taurog, J. D. (2009) Animal models of spondyloarthritis. *Adv. Exp. Med. Biol.* **649,** 245–254 CrossRef Medline
55. Büdinger, L., and Hertl, M. (2000) Immunologic mechanisms in hypersensitivity reactions to metal ions: an overview. *Allergy* **55,** 108–115 CrossRef Medline
56. Rowley, B., and Monestier, M. (2005) Mechanisms of heavy metal-induced autoimmunity. *Mol. Immunol.* **42,** 833–838 CrossRef Medline
57. Schiraldi, M., and Monestier, M. (2009) How can a chemical element elicit complex immunopathology? Lessons from mercury-induced autoimmunity. *Trends Immunol.* **30,** 502–509 CrossRef Medline
58. Illing, P. T., Vivian, J. P., Purcell, A. W., Rossjohn, J., and McCluskey, J. (2013) Human leukocyte antigen-associated drug hypersensitivity. *Curr. Opin. Immunol.* **25,** 81–89 CrossRef Medline
59. Schanda, P., Kupce, E., and Brutscher, B. (2005) SOFAST-HMQC experiments for recording two-dimensional heteronuclear correlation spectra of proteins within a few seconds. *J. Biomol. NMR* **33,** 199–211 CrossRef Medline
60. Kabsch, W. (2010) XDS. *Acta Crystallogr. D Biol. Crystallogr.* **66,** 125–132 CrossRef Medline
61. McCoy, A. J., Grosse-Kunstleve, R. W., Adams, P. D., Winn, M. D., Storoni, L. C., and Read, R. J. (2007) Phaser crystallographic software. *J. Appl. Crystallogr.* **40,** 658–674 CrossRef Medline
62. Adams, P. D., Afonine, P. V., Bunkoczi, G., Chen, V. B., Davis, I. W., Echols, N., Headd, J. J., Hung, L.-W., Kapral, G. J., Grosse-Kunstleve, R. W., McCoy, A. J., Moriarty, N. W., Oeffner, R., Read, R. J., Richardson, D. C., *et al.* (2010) PHENIX: a comprehensive Python-based system for macromolecular structure solution. *Acta Crystallogr. D Biol. Crystallogr.* **66,** 213–221 CrossRef Medline
63. Emsley, P., Lohkamp, B., Scott, W. G., and Cowtan, K. (2010) Features and development of Coot. *Acta Crystallogr. D Biol. Crystallogr.* **66,** 486–501 CrossRef Medline
64. Williams, C. J., Headd, J. J., Moriarty, N. W., Prisant, M. G., Videau, L. L., Deis, L. N., Verma, V., Keedy, D. A., Hintze, B. J., Chen, V. B., Jain, S., Lewis, S. M., Arendall, W. B., 3rd, Snoeyink, J., Adams, P. D., *et al.* (2018) MolProbity: More and better reference data for improved all-atom structure validation. *Protein Sci.* **27,** 293–315 CrossRef Medline
65. DeLano, W. L. (2002) *The PyMOL Molecular Graphics System* http://www.pymol.org
66. Loll, B., Rückert, C., Hee, C. S., Saenger, W., Uchanska-Ziegler, B., and Ziegler, A. (2011) Loss of recognition by cross-reactive T cells and its relation to a C-terminus-induced conformational reorientation of an HLA-B*2705-bound peptide. *Protein Sci.* **20,** 278–290 CrossRef Medline

Metal-triggered conformational reorientation of a self-peptide bound to a disease-associated HLA-B*27 subtype

Ronja Driller, Martin Ballaschk, Peter Schmieder, Barbara Uchanska-Ziegler, Andreas Ziegler and Bernhard Loll

J. Biol. Chem. 2019, 294:13269-13279.
doi: 10.1074/jbc.RA119.008937 originally published online July 11, 2019